

Near-barrier fusion reactions induced by α on ^{197}Au , ^{193}Ir , ^{191}Ir , ^{185}Re , ^{181}Ta , ^{121}Sb and ^{69}Ga nuclei

M ISMAIL

Variable Energy Cyclotron Centre, I/AF, Bidhan Nagar, Calcutta 700 064, India
Email: ismail@veccal.ernet.in

MS received 6 March 1998; revised 24 August 1998

Abstract. Fusion-evaporation cross-sections for the α -induced reactions upon ^{197}Au , ^{193}Ir , ^{191}Ir , ^{185}Re , ^{181}Ta , ^{121}Sb and ^{69}Ga nuclei at bombarding energies near the Coulomb barrier have been measured by off-line observation of the γ -rays emitted in the radioactive decay of the residual nuclei using stacked foil technique. The total fusion cross-section for the systems have been compared with simple statistical model calculations using the code ALICE/91 as well as with the coupled channel calculations that include the β_2 and β_4 static deformations and dynamic couplings of the vibrational/rotational states of the target and the projectile using the code CCDEF.

Keywords. α -induced reaction on Au, Ir, Re, Ta, Sb and Ga; near-barrier fusion reaction; Alice/91 and CCDEF codes.

PACS Nos 25.70; 24.10

1. Introduction

The observation of the large enhancements of fusion cross-section near and below the Coulomb barrier in a great number of reactions between heavy ions compared with the predictions of the conventional one dimensional barrier penetration model has accelerated the exploration of how nuclear structure influences the nuclear process [1] and [2] near the Coulomb barrier. Considerable progress has been made in understanding the enhancement of the fusion cross-section by including new degrees of freedom such as static and dynamic deformations of both target and projectile and nucleon transfer. These effects reveal an interesting interplay between the dynamics of the reaction and the structure of the participant nuclei [1], [2], and [3].

The reactions we have studied are the α -induced reactions on ^{197}Au , ^{193}Ir , ^{191}Ir , ^{185}Re , ^{181}Ta , ^{121}Sb and ^{69}Ga nuclei near the Coulomb barrier. The neutron evaporation is the main decay mode of the compound nuclei produced at near-barrier energies for these reactions. The evaporation residues produced in these reactions are radioactive having half-lives of a few hours to a few days. It is therefore possible to use stacked foil techniques to determine the fusion cross-sections for these systems by measuring individual channel cross-sections. The intention of these studies is to understand the enhancement of any of the α -induced total fusion cross-section by including new degrees of freedom such as static and dynamic deformations of both target and projectile and

nucleon transfer. Section 2 describes the experimental procedure and the results are being presented in § 3. Section 4 summarizes the conclusions.

2. Experimental procedure

The fusion excitation functions for the α -induced reactions upon ^{197}Au , ^{193}Ir , ^{191}Ir , ^{185}Re , ^{181}Ta , ^{121}Sb and ^{69}Ga nuclei were determined using the absolute yields of characteristic γ -rays pertaining to the decay of each radioactive residual nuclides using the stacked foil technique. The targets of gold, iridium, rhenium and tantalum foils (99.9% pure commercially available) were thin self supporting foils and the thicknesses were 4.8 μm , 13.0 μm , 25.0 μm and 10.5 μm respectively obtained by weighing. The targets for Ga and Sb were prepared by vacuum evaporation of (99.9% pure commercially available) gallium nitrate and antimony trioxide respectively on 23.4 μm aluminum backings (30 mm in diameter). The targets of iridium, rhenium, antimony and gallium were not enriched and the procedure for extracting the cross-sections for individual isotopes are explained in ref. [4] and [6]. The average thickness of gallium and antimony targets were $\approx 1.0 \text{ mg/cm}^2$ and $\approx 2.0 \text{ mg/cm}^2$ respectively. The average thickness of the target and degrader foils were determined by weighing. No degraders were used for the gold, iridium, rhenium and tantalum stacks. For the gallium and antimony stacks 23.4 μm thick aluminum backings were used as degrader foils. Each foil was cut out into a square shape and pasted over an annular aluminium ring having 30.0 mm as outer diameter. The stacks were irradiated in a chamber (as shown in figure 1 of ref. [4]) specially constructed for this purpose. The stacks were exposed to the unanalyzed external beam from the 224 cm variable energy cyclotron in Calcutta. The beam current on the targets was kept below 200 nA for the metallic foils and below 100 nA for gallium and antimony targets. The total α -particle beam was collected and measured using a calibrated ORTEC current integrator. The unanalyzed beam energy resolution was $\approx 0.2 \text{ MeV}$. The accuracy in absolute energy is expected to be $\approx 0.5 \text{ MeV}$. However from some of the excitation functions for the α -induced reactions on various targets the energies were re-calibrated with respect to their thresholds and thereby improving the accuracy in absolute energy to better than 0.5 MeV.

The mean beam energy at the half-thickness of each target of a stacked foil assembly was calculated from the energy degradation of the initial beam energy according to the given stopping power values for the different materials. We have used the stopping powers from the tabulated values of Williamson *et al* and Hubert *et al* [5]. The γ -rays emitted by the activated foils were detected with a HPGe detector (having 30% efficiency) available at our centre (VECC). In most of the cases the γ -rays, used in yield determination stand out very prominently in the spectra and did not pose any identification problem. One representative γ -ray spectrum from $^{197}\text{Au} + \alpha$ reaction at $E_\alpha = 21.0 \text{ MeV}$ is shown in figure 1. The efficiency calibrations of the detector were done with a standard ^{152}Eu . The nuclear data necessary for the evaluation of the cross-sections are presented in table 1 of ref. [4] and [6]. The half-lives of the radioactive atoms, the γ -rays energies and branching ratios were taken from the chart of the nuclides and table of isotopes [7]. In table 1 of ref. [4] and [6] only those γ -rays are listed which were chosen for the calculation of the cross-sections. The reaction Q -values were calculated by using the atomic mass

Near-barrier fusion reactions

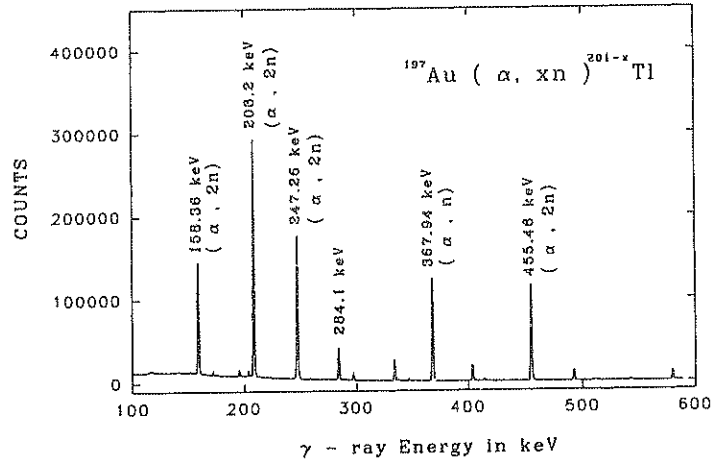


Figure 1. Offline γ -ray spectrum obtained with a high purity germanium (HPGe) intrinsic detector for $^{197}\text{Au} + \alpha$ at laboratory bombarding energy ($E_\alpha = 21.0\text{ MeV}$) showing the relevant delayed γ -ray emitted from the radioactive residues.

Table 1. Parameters used in CCDEF calculations for induced reactions. The first five rows indicate the input parameters associated with the targets. The next three rows are the potential parameters for the uncoupled case. V and R are Coulomb barrier and corresponding Coulomb radius. The last four rows are the reaction Q -values in (MeV).

Target Parameters	^{197}Au	^{193}Ir	^{191}Ir	^{185}Re	^{181}Ta	^{121}Sb	^{69}Ga
β_2	0.120	0.188	0.170	0.200	0.250	0.106	0.214
E_x (MeV)	0.426	0.120	0.206	0.155	0.104	1.165	1.028
β_3	0.073	0.060	0.070	0.065	0.050	0.140	0.290
E_x (MeV)	2.486	1.433	1.378	1.414	1.374	2.401	2.561
DV	12.5	25.0	5.0	25.0	10.0	30.0	7.5
V_b (MeV)	20.367	19.414	20.450	19.024	19.259	13.859	9.803
R_b (fm)	10.453	10.727	10.109	10.656	10.195	9.906	8.391
$\hbar\omega$ (MeV)	5.249	5.176	5.137	5.151	5.132	4.614	4.122
V_{cb} (MeV)	20.375	20.917	20.959	20.499	20.078	15.126	10.137
R_{cb} (fm)	10.644	10.602	10.581	10.537	10.471	9.711	8.807
$Q(\alpha, n)$	-09.736	-09.024	-10.084	-10.150	-09.873	-07.869	-06.741
$Q(\alpha, 2n)$	-16.813	-15.670	-16.944	-16.482	-16.340	-15.370	-15.147
$Q(\alpha, 3n)$	-25.434	-24.054	-25.709	-24.663	-24.784	-25.305	-26.771
$Q(\alpha, 4n)$	-32.606	-30.914	-32.697	-31.355	-31.746	-33.188	-36.103

table of Wapstra and Audi [8]. For details of experimental procedures please refer to Ismail [4].

3. Experimental results

The excitation functions for the (α, n) , $(\alpha, 2n)$ and $(\alpha, 3n)$ nucleon evaporation channels were measured for the alpha induced reactions on ^{197}Au , ^{193}Ir , ^{191}Ir , ^{185}Re , ^{181}Ta , ^{121}Sb and

^{69}Ga nuclei. At the barrier energies only neutron channels dominate the evaporation residue cross-sections. The systematic uncertainties associated with the beam energy resolution and fluctuations do not allow very accurate determination of absolute total fusion cross-sections. At energies near the Coulomb barrier only (α, n) , $(\alpha, 2n)$ and $(\alpha, 3n)$ channels dominate the fusion cross-section and the sum

$$\sigma_T = \sum_{i=1}^{i=3} \sigma_{in} \quad (1)$$

exhausts the fusion cross-section almost completely. The threshold energies of $(\alpha, 4n)$ and $(\alpha, 5n)$ channels are much above the Coulomb barrier as seen from table 1 and hence these were not considered in the computation of σ_T . The errors in the fusion cross-sections resulting from the sum of (α, n) , $(\alpha, 2n)$ and $(\alpha, 3n)$ cross-sections are of the order of 15% which however does not take into account the systematic errors arising from beam energy resolution and fluctuations.

In the present case the projectile is spherical as well as having no vibrational or rotational states. Therefore only the static deformation of the target as well as dynamic coupling of its vibrational or rotational states (as the case may be) are taken into account. We have used the coupled channel code CCDEF [9] as well as statistical model code ALICE/91 [10] to calculate the theoretical cross-section for comparison with experimental data.

In the no-coupling no-deformation mode (uncoupled mode) the CCDEF code calculates fusion cross-sections from a Christensen–Winther type potential [11]. There is only one free parameter DV (the potential depth) in the calculation which is obtained by a best fit procedure in the energy region above the Coulomb barrier. The potential depth parameter DV obtained in this way is kept fixed for the calculations with other coupled channeled calculations. The optimized potential depth parameters DV along with the corresponding derived quantities V_b , R_b (the height and position of the unperturbed barrier respectively) and $\hbar\omega$ (a measure of the thickness of the barrier) are presented in table 1. The other parameters, the Coulomb barrier $V_{cb}(= 1.44Z_p Z_T / R_{cb})$ and the corresponding Coulomb radius R_{cb} are presented in table 1. The Coulomb barriers are shown as inverted triangles in figures 2(a) and 2(b). The expression for the radius of a Coulomb barrier as obtained by Christensen and Winther [11] by straight line fit is given below

$$R_{cb} = 1.07[(A^{1/3})_p + (A^{1/3})_T] + 2.72. \quad (2)$$

In the mode where the permanent nuclear deformations are explicitly considered, the Coulomb interaction depends on the orientation of the deformed nuclei. The nuclear form factors for the vibrational excitations, which are proportional to the derivative of the deformed potential are calculated for each orientation of the target and the projectile. The total fusion cross-section are then constructed by averaging the results of the coupled channel calculations over all relative orientations of the deformed systems [12].

Figures 2(a) and 2(b) show the fusion excitation function versus centre-of-mass energy for the systems $^{197}\text{Au} + \alpha$, $^{193}\text{Ir} + \alpha$, $^{191}\text{Ir} + \alpha$, $^{185}\text{Re} + \alpha$, $^{181}\text{Ta} + \alpha$, $^{121}\text{Sb} + \alpha$ and $^{69}\text{Ga} + \alpha$. The filled circles are the experimental points. Since the error bars are of the size of the symbols in most of the cases, they are not visible. (i) The dotted curves are the results of CCDEF fits with all the couplings turned off i.e. for spherical colliding nuclei. (ii) The short-dashed line curves are the CCDEF fits using surface

Near-barrier fusion reactions

coupling terms only i.e. when only the excited vibrational or rotational states of the target nuclei are considered. (iii) The long dashed line curves are the simplified coupled channeled CCDEF code fits when we consider in addition to coupled vibrational or rotational states of the target nuclei, the permanent quadrupole deformation of the targets also. The parameters of the calculations are presented in table 1. The deformation parameters β_2 and β_3 and their excitation energies were obtained from the ref. [13] and [14]. Since the projectile is spherical as well as not very heavy and the targets are also not very deformed though heavy, all the three sets mentioned above fit the experimental data fairly well. However the third set fits the experimental data better than the first two sets.

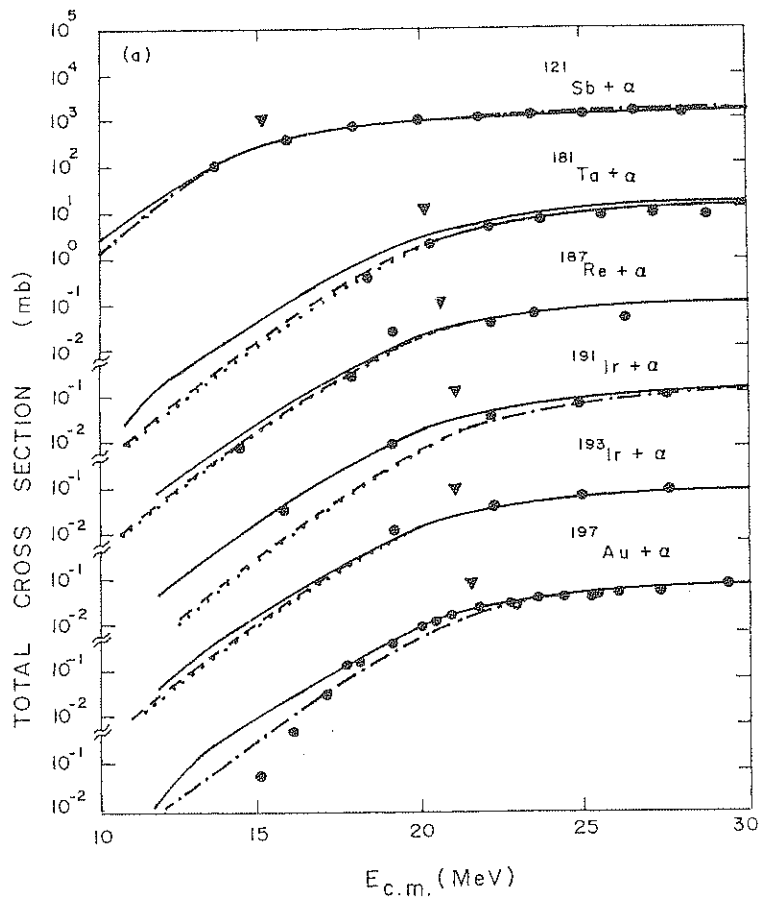


Figure 2(a). Fusion excitation function versus centre-of-mass energy for the systems $^{197}\text{Au} + \alpha$, $^{193}\text{Ir} + \alpha$, $^{191}\text{Ir} + \alpha$, $^{185}\text{Re} + \alpha$, $^{181}\text{Ta} + \alpha$ and $^{121}\text{Sb} + \alpha$. The filled circles are the experimental points. The solid curves are the ALICE/91 code fits. The long dashed curve is the CCDEF code fits using the parameters shown in table 1. The short-dashed curves are the CCDEF fits using surface coupling terms only. The dotted curves are the results of CCDEF fits with all the couplings turned off. The inverted triangles are the Coulomb barrier V_{cb} (MeV).

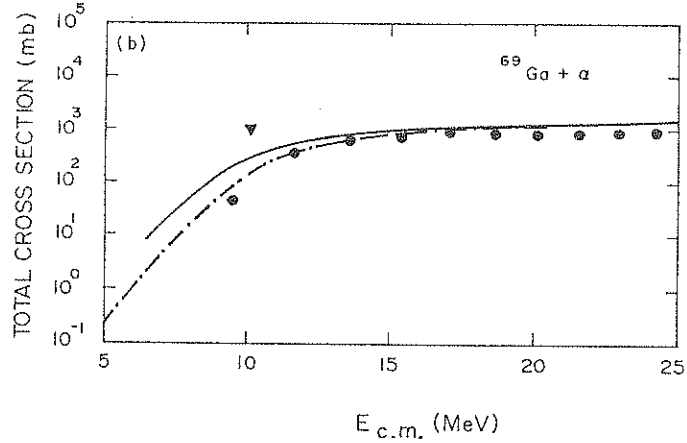


Figure 2(b). Same as figure 1(a) but for the system $^{69}\text{Ga} + \alpha$.

In figures 2(a) and 2(b) the solid curves are the ALICE/91 code [10] fits. The ALICE/91 code [10] describes the process of equilibrium evaporation of particles and γ -rays in terms of the Weisskopf and Ewing model [10] and pre-equilibrium reaction mechanism according to the hybrid and geometry dependent hybrid model [10]. We have used the option in the default version of GDH whereby only the first collision is localized according to the impact parameter (Blann and Vonach [15]) with all the higher order precompound terms being treated by the hybrid model i.e. using nuclear densities averaged over the nucleus and independent of impact parameter. We have taken an initial exciton configuration $n_0 = 4$ ($n_n = 2, n_p = 2, n_h = 0$) which is equivalent to break-up of the incoming α -particle in the field of the nucleus and the nucleons occupying excited states above the fermi energy gives a better description of the excitation function compared to other configurations for the α -particle bombarding energies up to 60.0 MeV. In figures 2(a) and 2(b), the solid curves are the above mentioned geometry dependent hybrid fits. The statistical model parameters used in the above fits were the same as those used for fitting the excitation functions for individual channels as described in Ismail [4] for α -induced reactions on ^{121}Sb and ^{69}Ga nuclei and in ref. [6] for α -induced reactions on ^{197}Au , ^{193}Ir , ^{191}Ir , ^{185}Re , and ^{181}Ta nuclei.

It is now well established that fusion cross-sections at sub-barrier energies may be enhanced by several order of magnitude compared with the predictions of a one dimensional potential model, which is due to *coupling* of the relative motion to nuclear intrinsic degrees of freedom [1]. In the linear coupling approximation the coupling strength F [3] at the barrier position r_B of the bare Coulomb barrier is given by

$$F = (\beta_\lambda / \sqrt{4\pi}) Z_p Z_T e^2 \left\{ -R_T^{(0)} / r_B^2 + (3 / (2\lambda + 1)) (R_T^{(0)})^\lambda / r_B^{\lambda+1} \right\} \quad (3)$$

where $R_T^{(0)}$ is the equivalent radius of the target nucleus, λ is the multipolarity of the phonon excitation and β_λ is the deformation parameter. The coupling strength is proportional to the product of $Z_p Z_T$. For very asymmetric systems the product of the charges $Z_p Z_T$ is relatively small. Therefore the coupling strength in asymmetric systems is several times smaller than in symmetric systems, even though the values of deformation

parameter β_λ are similar. Another reason that the enhancement of the fusion cross-section is small in very asymmetric systems is its small reduced mass. In the WKB formula for the barrier penetrability, the reduced mass parameter appears in the exponent. Hence larger the reduced mass, the more sensitive the penetrability to the slight change of the potential. That is why the result in the linear coupling approximation show a relatively small enhancement of the fusion cross-section compared with the no-coupling limit. That is why the data show comparable agreements with statistical model code Alice as well as with simplified coupled channel calculation using the code CCDEF.

4. Conclusions

We have analysed the behaviour of the fusion excitation functions for the systems $^{197}\text{Au} + \alpha$, $^{193}\text{Ir} + \alpha$, $^{191}\text{Ir} + \alpha$, $^{185}\text{Re} + \alpha$, $^{181}\text{Ta} + \alpha$, $^{121}\text{Sb} + \alpha$ and $^{69}\text{Ga} + \alpha$ using the codes CCDEF [9] and ALICE/91 [10]. The simplified coupled-channel calculations show that the near barrier excitation functions could be understood by coupling of the permanent quadrupole deformation as well as coupling of the vibrational or rotational states of the targets. For the systems studied in this paper the statistical model code also fits the total fusion cross-section fairly well.

Acknowledgements

We sincerely thank Dr M Blann for supplying the ALICE/91 code and Dr S Landowne for supplying the CCDEF code.

References

- [1] M Beckerman, *Phys. Rep.* **129**, 145 (1985)
- [2] S Steadman and M Rhoades-Brown, *Ann. Rev. Nucl. Sci.* **36**, 649 (1986)
- [3] R Vandenbosch, *Ann. Rev. Nucl. Sci.* **42**, 447 (1992)
- [4] M Ismail, *Phys. Rev.* **C41**, 87 (1990)
- [5] C F Williamson, J P Boujot and J Picard, CEA-R 3042 (1966)
F Hubert, R Bimbot and H Gavin, *Atomic Data and Nucl. Data Tables* **46**, 1 (1990)
- [6] M Ismail, *Pramana – J. Phys.* **50**, 173 (1998)
- [7] C M Lederer and V S Shirley, *Table of isotopes*, 7th edition (New York: John Wiley, 1978);
V Osorio and H Peraza, *IAEA-NDS-161*, June 1995
- [8] A H Wapstra and G Audi, *Nucl. Phys.* **A432**, 1 (1985)
- [9] J Fernandez-Niello, C H Dasso and S Landowne, *Comput. Phys. Commun.* **54**, 409 (1989)
- [10] M Blann, ALICE/1991: Evaporation Code, Lawrence Livermore National Lab, University of California, Livermore UCID-20169 (1985)
- [11] P R Christensen and A Winther, *Phys. Lett.* **B65**, 19(1976)
- [12] C Y Wong, *Phys. Rev. Lett.* **31**, 766 (1973)
- [13] S Raman, C Malarkey, W Milner, C Nestor Jr. and P Stelson, *Nucl. Data Tables* **36**, 1 (1987)
- [14] R Spear, *Nucl. Data Tables* **42**, 55 (1989)
- [15] M Blann and H K Vonach, *Phys. Rev.* **C28**, 1475 (1983)

